

Article

Evaluation of the Accuracy of the Identified Equivalent Electrical Circuit of LiPePO₄ Battery through Verified Measurements

Michal Frivaldsky * and Marek Simcak

Department of Mechatronics and Electronics, Faculty of Electrical Engineering and Information Technology, University of Zilina, 010 01 Zilina, Slovakia; marek.simcak@feit.uniza.sk

* Correspondence: michal.frivaldsky@feit.uniza.sk

Abstract: In this paper, the system procedure for the identification of the equivalent electrical circuit diagram of electrochemical cells is being given. Due to the fact that energy storage systems (ESS) penetrate within many applications, the availability of their accurate and simple simulation models for time-domain analysis is very desirable. This paper describes the configuration of the laboratory measuring systems required for data acquisition, curation, and analysis of received measured data required for development of equivalent electrical circuit models (EECM) of electrochemical cells. Nowadays, various types of electrochemical cells are available for packaging technology. Therefore, the evaluation of presented identification methodology is validated through measurements of two different types of LiFePO₄ cells. The first cell type is prismatic labeled LFP040AHA, and the second type is NPB 60 AH of the same manufacturer. The main aim of this paper is the determination of the elements of equivalent electrical circuit schematics of selected electrochemical cells. Consequently, the development of a simulation model is described, together with the evaluation of its accuracy through comparisons with experimental measurements. From achieved results, the relative error of simulation model varies at 2%, and thus the presented methodology is suitable for identification of EECM, and consequent design of accurate and fast computing simulation models of ESS systems.



Citation: Frivaldsky, M.; Simcak, M. Evaluation of the Accuracy of the Identified Equivalent Electrical Circuit of LiPePO₄ Battery through Verified Measurements. *Batteries* **2022**, *8*, 38. <https://doi.org/10.3390/batteries8050038>

Academic Editors: Carlos Ziebert and Seiji Kumagai

Received: 20 January 2022

Accepted: 13 April 2022

Published: 22 April 2022

Publisher's Note: MDPI stays neutral with regard to jurisdictional claims in published maps and institutional affiliations.



Copyright: © 2022 by the authors. Licensee MDPI, Basel, Switzerland. This article is an open access article distributed under the terms and conditions of the Creative Commons Attribution (CC BY) license (<https://creativecommons.org/licenses/by/4.0/>).

1. Introduction

Today, much of the industry is beginning to adapt to the advent of electromobility. In other words, society is pushing to produce energy from renewable sources and to use it efficiently. These aspects determine that developments in the field of energy storage systems are beginning to flourish. The development of new chemicals, battery management systems, or the maximization of battery safety opens the door for development in this research area. The production of batteries is experiencing a significant boom. Many manufacturers are trying to supply new types of batteries, new packaging, or parameter improvements. Development requires battery parameters, which the manufacturer rarely states. Therefore, development needs a system that can detect these parameters. Energy storage systems composed of batteries are nowadays increasingly gaining popularity within industrial applications requiring high power and high voltage rankings. This is due to their advantageous features, such as high operational efficiencies and low environmental impact when compared to fossil fuels. Currently, it is possible to discover several battery technologies, while electrochemical cells based on Li-ion are typically the preferred solutions due to their specific energy density and acceptable operational life [1,2].

To maximize battery performance, an effective battery simulation model plays a crucial role in supporting the system design, its functional analysis, and control strategies. Considering current battery model types—electrochemical models, reduced order models,

and data-driven black-box models—the equivalent electrical circuit models (EECMs) offer acceptable accuracy of the results related to expected battery operation. In this way, it is possible to analyze power prediction, estimate the state of charge and state of health as well. An additional advantage of the use of such models is the possibility to evaluate balancing methods during charging and discharging procedures [3–5].

Due to the abovementioned facts, the proposal and design of the system of parameter identification of an equivalent electrical circuit of electrochemical cells is required. Basically, this statement can be confirmed by the fact that almost all manufacturers provide electrical parameters for their batteries, while the parameters corresponding to the element of the equivalent circuit are not subject to publication in the product datasheets.

According to the dynamic behavior of the battery cell, the ECM is composed from resistances, capacitances, and a voltage source [6,7]. In order to model open-circuit voltage (V_{oc}), the ideal voltage source or capacitor is being utilized within the simulation model. The other components of the circuit simulate the dynamic effects such as terminal voltage relaxation and battery internal resistance [8–11]. Based on the manufacturer datasheet information, it is possible to determine the maximum current load of the cell, while this parameter is directly related to the internal resistance of the cell. The internal resistance of the cell is only rarely mentioned by the manufacturer. At the same time, this parameter is very important when considering the maximum operational power of the cell, whereby it is directly related to temperature variation of the cell itself. Considering battery safety management, the value of internal resistance indirectly influences safety conditions, in the way of voltage drop during battery loading. Voltage drop cannot reach the value of safe minimum voltage level (mainly for lithium-based cells) [12–14].

Based on the previous description, it is desirable to be able to identify ECM of electro-chemical cells in order to evaluate the operational performance of energy storage systems. In other words, various operational scenarios of cell itself can be identified, or investigation of battery packs can be carried out, and modules can be better optimized with the use of accurate and fast computing simulation models. Moreover, analysis can be performed considering cooperation with charging/discharging systems, i.e., power electronic systems equipped by ESS can actually be evaluated. Based on previous facts, the paper presents description of the system configuration together with description of the identification methodology and consequent simulation model development based on ECM of selected lithium-based cells. The results show that the methodology enables to identify parameters of ECM in dependency of SOC, while compared to experimental results, the accuracy of proposed methodology reaches max. 5% of the relative error.

2. System Configuration for the Identification of ECM of the Battery

A block diagram of the proposed identification algorithm using system configurations of laboratory measuring devices is shown in Figure 1. The main principle of the operation is based on the control of a programmable load and a programmable power supply unit. For this main equipment, a special control algorithm was designed using an automated data measurement and recording system through LabView environment (setting of the charging and discharging parameters—voltage, current, power). At the same time, the cell temperature is monitored, and in case of high temperature, the control system switches off the procedure for ECM identification. The main control element is represented by PXI 1031, in which two cards PXI 4070 and PXI 8101 are connected [15]. The measuring card PXI 4070 represents a very precise multimeter. This card monitors the voltages directly on the cell and the voltage change of the thermistor, which is the thermal sensor. The PXI 8101 control card is the interface between the PC and the load/power supply. This card includes an HDMI port for connecting a display, USB ports for a mouse keyboard, and serial communication with a programmable power supply and load. These programmable devices are controlled via this serial communication. The investigation electrochemical cell is placed within special chamber, where terminals of power supply and load are connected.

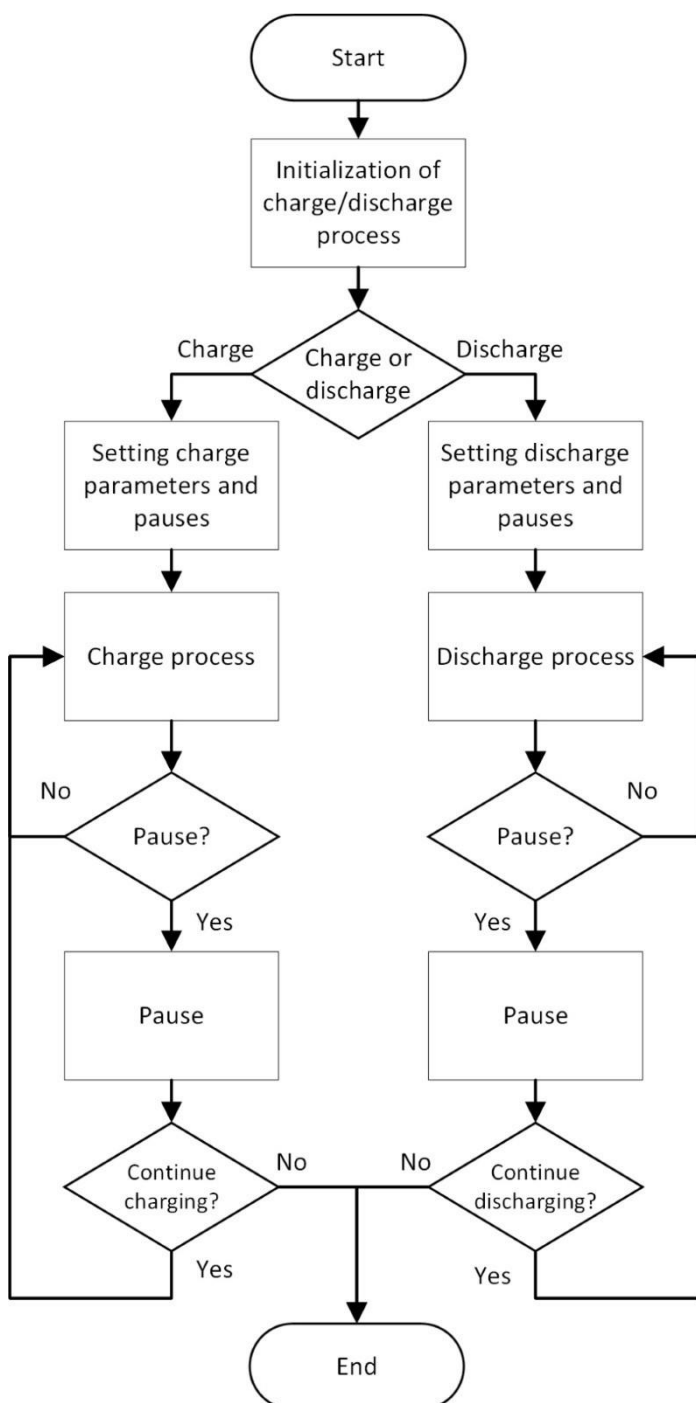


Figure 1. Algorithm used within identification procedure of parameters of EECM.

The principal electrical schematics of measurement set-up related to the described algorithm is shown on Figure 2, while the experimental laboratory set-up is shown in Figure 3. This system is adapted to be able to log measured values even during charging or discharging process, and also during battery relaxation. The identification algorithm is defined by these relaxation periods that allow it to evaluate values of RC networks responsible for short and long dynamic actions of electrochemical cells. The experimental set-up is equipped by the abovementioned power supply unit and electronic programmable load, while its main properties are summarized in Tables 1 and 2. KIKUSUI PLZ1004W is a programmable load. This load works up to a power of 1 kW, a maximum voltage of 150 V, and a maximum current of 200 A. EA-PSI 8080-60 is a programmable power supply.

This power supply can work up to 1.5 kW, maximum voltage 80 V, and maximum current 60 A. The last part of the laboratory set-up is a measuring chamber, where terminals for the battery are placed; it also contains battery racks, a thermistor, a webcam, and a mechanical disconnector. It is also adapted for testing electrochemical cells within critical operational conditions (short circuit, deep discharge, overcharging, etc.) [16,17].

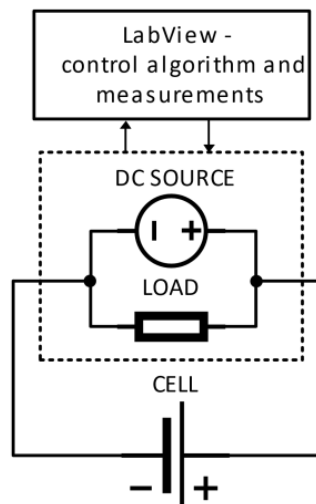


Figure 2. Principal electrical schematic of measurement set-up for EECM identification.

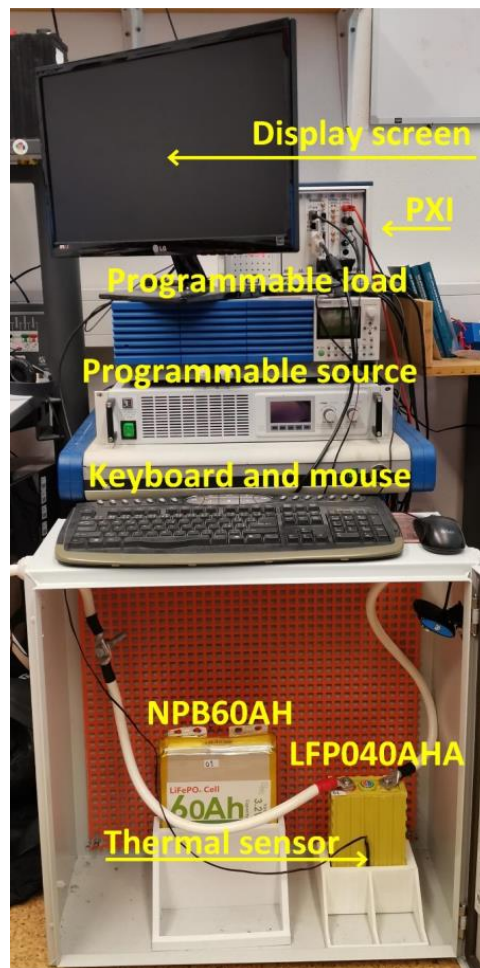


Figure 3. Implementation of the identification of the equivalent replacement battery scheme.

Table 1. Main properties of programmable load KIKUSUI PLZ1004W.

Maximum Operating Current	200 A
Operating voltage	1.5–150 V
Power	1000 W
Communication interface	GPIB, RS232C, USB
Working modes	CC, CR, CP, CV

Table 2. Main properties of programmable source EA-PSI 8080-60.

Maximum operating current	60 A
Operating voltage	0–80 V
Power	1500 W
Efficiency	92%
Communication interface	GPIB, RS232, USB, CAN
Protection	OV, OT

3. Description of Identification Process Procedure

3.1. Charging Process

During charging, the algorithm sets the maximum value of voltage, charging current, and charging power, while the current control mode is set. This mode ensures that there will never be a situation where the voltage of the source can overcharge the cell or damage it with higher voltage applied. In other words, if the maximum value of the voltage is achieved by a slow rise, the value of the current is automatically reduced. Then, the source switches from current control mode to voltage control mode. During battery charging, the cell voltage is monitored by a special measuring card—PXI 4070—with high resolution and measurement accuracy, which is required due to the cell voltage level and the need for the smallest possible error. The charging process is defined in the way that after charge of the 1/10 of the battery capacity, the procedure passes into relaxation stage. This is repeated 10 times, each time after charging 1/10 of the battery capacity. In this way, the dependency of EECM parameters on SOC are identified [15–17].

3.2. Discharging Process

During the discharging process, the algorithm sets the amount of discharge current, the capacity at which the discharge ends, and the value of the deep discharge voltage of the electrochemical cell. Setting the value of the deep discharge is important when full SOC range is accomplished [18,19]. Therefore, a fully charged cell is discharged to a voltage level of 2.5 V. This ensures that the discharge characteristic is entirely completed. Similarly to the charging process, the algorithm here is preset to adopt relaxation periods when 1/10 of the cell capacity is discharged. The process is repeated 10 times to be able to identify dependency of RC components for the whole range of SOC [20,21].

3.3. Analysis of Measurement Data

The measured data consist of four values, which are logged every second:

- the value of the current flowing through the cell,
- the cell voltage,
- the power currently sunk/sourced from battery,
- and the value of the amount of capacity.

A crucial task during measurement is to precisely identify time-dependency of the relaxation period to be consequently able to accurately estimate values of equivalent electrical circuit model components (Figure 4).

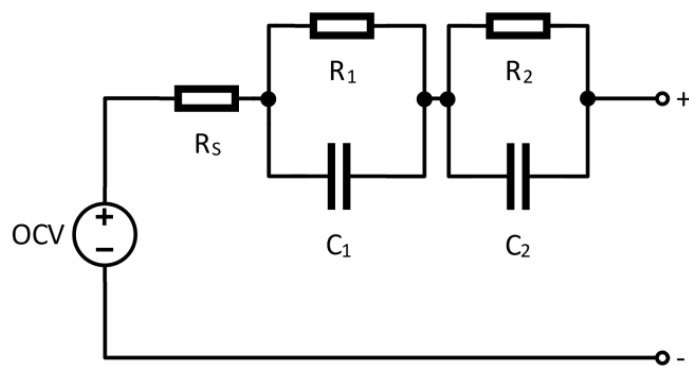


Figure 4. Equivalent electrical circuit model of electrochemical cell (RR2C2).

Figure 5 shows the example of one relaxation period, while the duration is reflected from the time constants of RC networks. Time instant t_0 is the time before the battery passes to the relaxation period, t_1 is the time instant related to switch-off action of the load, t_2 is the instant for the end of relaxation after the load is switched off (short relaxation) and t_3 is the time after passing 600 s (long relaxation).

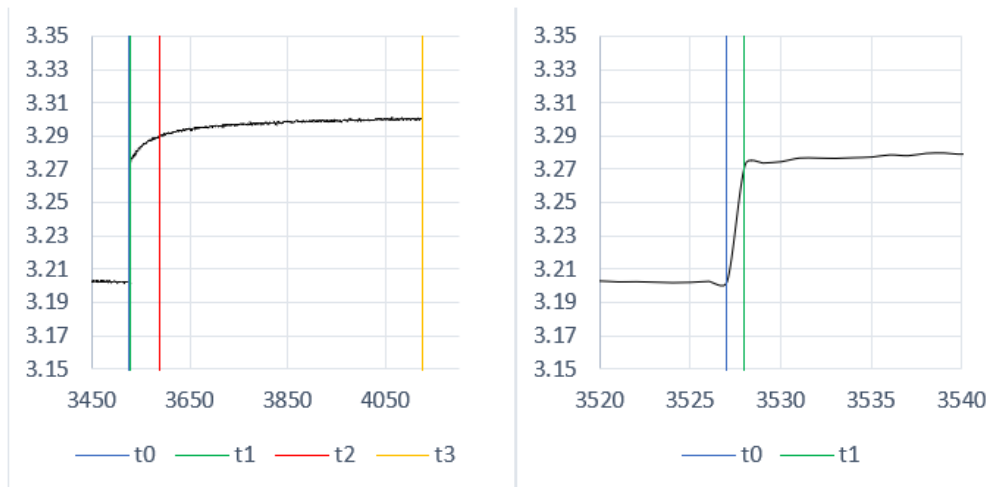


Figure 5. Example of analysis of regenerated cell voltage (**left side**—one pulse, **right side**—pulse zoomed at time t_0 and t_1).

The voltage difference between t_0 and t_1 determines the value of the internal resistance of the cell. This is represented by voltage V_0 (1). Considering EEM, this represents the parameter R_s in Equation (4). As was already mentioned, the voltage difference between t_1 and t_2 and the voltage difference between t_2 and t_3 represent a fast and a slow time constant; this corresponds to the values of voltage V_1 (2) (fast) and V_2 (3) (slow). Related to fast time constant, components C_1 and R_1 are forming this network, and Equations (5) and (7) should be used for their calculation. The slow time constant is represented by parameters C_2 and R_2 , while Equations (6) and (8) shall be used for identification. Related to the dependency on SOC, the values of components of EECM are evaluated for the whole range of SOC with the step of 10%.

$$V_0 = V_{t1} - V_{t0} \quad (1)$$

$$V_1 = V_{t2} - V_{t1} \quad (2)$$

$$V_2 = V_{t3} - V_{t2} \quad (3)$$

$$R_s = \frac{V_0}{I} \quad (4)$$

$$R_1 = \frac{V_1}{I} \quad (5)$$

$$R_2 = \frac{V_2}{I} \quad (6)$$

$$C_1 = \frac{t_2 - t_1}{R_1} \quad (7)$$

$$C_2 = \frac{t_3 - t_2}{R_2} \quad (8)$$

3.4. Selected Battery Technology Undergoing Parameters Identification

LiFePO₄-based electrochemical cells were used to verify the system methodology. Selected cells were from the same manufacturer, Winston, while the main difference was related to the package. The manufacturer declared parameters shown in Tables 3 and 4. As can be seen, parameters required for modelling the equivalent electrical circuit schematics are not mentioned; while considering development, design, and investigation of behavior of the high-voltage battery pack, the parameters of EECS are more than important.

The first cell LFP040AHA is a cell using a prismatic package. The second cell NPB60AH is provided with a pouch package. Both cells have similar operating voltages, while power capability differs [22–24].

3.4.1. WINSTON LFP040AHA

This cell is based on cathode type LiFePO₄. The manufacturer declares better temperature stability than Li-ion (LiCoO₂) cells. However, better thermal stability of the cell is at the expense of lower energy density. The prismatic package of this cell is designed to make it easier to construct high-voltage battery packs. The parameters defined by the manufacturer are shown in Table 3 [5].

Table 3. Parameters of cell LFP040AHA.

Parameters	Values
Nominal voltage	3.3 V
Capacity	40 Ah
Deep discharge voltage	2.5 V
Maximum charging voltage	4 V
Optimal charging/discharging current	20 A (0.5 C)
Maximum discharge current	120 A (3 C)
Maximum peak discharge current	400 A (10 C) in 5 s
Maximum working temperature	80 °C

3.4.2. WINSTON NPB 60 AH

Like the previous cell, this cell has a cathode made of LiFePO₄ material. The main difference compared to the previous cell is in the package (pouch type) and the higher capacity. The pouch type cell package does not have a pressure relief valve. Its construction allows the cell to inflate, thus the evaporated electrolyte does not leave the cell. This is an advantage over the previous type, because in the critical state, the electrolyte remains in the cell, thus not losing much capacity when reused. The great disadvantage of this cell is that the high-voltage batteries disassembled from this type of cell must consider that the packaging allows the cell to inflate. This results in higher space and hardware requirements. The parameters declared by the manufacturer are shown in Table 4 [6].

Table 4. Parameters of cell NPB 60 AH.

Parameters	Values
Nominal voltage	3.2 V
Capacity	60 Ah
Deep discharge voltage	2.5 V
Maximum charging voltage	3.8 V
Optimal charging/discharging current	18 A (0.3 C)
Maximum discharge current	60 A
Maximum working temperature	50 °C

4. Experimental Results and Their Verification

The identification of the parameters of EECM was carried out as described at Figure 1. The discharge was performed by setting the constant current value to 0.25 C. This value represents a current value that is low enough to be able to regenerate the cell voltage in a relatively short time and to ensure the voltage drop is not too high. For LFP040AHA it refers to 10 A, and for NPB 60 AH to 15 A. At every 10% SOC of the cell, the relaxation period was applied, so the cell voltage regeneration was monitored, and after a certain time it started to discharge within next 10% SOC cycle. This procedure was repeated until the cell dropped below 2.5 V.

The charging process was similar to discharging, thus the constant current value, maximum cell voltage, and charging steps reflecting 10% of SOC cycle were set. The result of this measurement was received as a characteristic of OCV in dependency on SOC, while it was received by approximation of the peaks of the regenerated voltages. The recovered voltages were approximated and compared with the mean of the voltage differences when discharging and charging a particular cell. In this way, an open circuit voltage (OCV) was expressed.

The capacity characteristic was constructed for a better approximation of the recovered voltages. This characteristic consists of two waveforms: charging progress (blue) and discharging progress (orange). This characteristic represents a waveform in the range from 0% to 100% of the SOC of a given cell. Therefore, the charging characteristic goes from left to right, and the discharging characteristic goes from right to left. The capacity of 0 Ah represents 0% SOC, and the end of the characteristic represents 100% SOC.

The time characteristic was created for the analysis of individual relaxation periods, as these are necessary for identification of the parameters of EECM. The analysis of these elements is shown in more detail in the article below. From these characteristics, it is seen that the end times of charging and discharging parts are not the same. As a result, the cell is charged in the CC (current control) mode. When the cell reaches the maximum set current value, the current must naturally decrease. As a result, charging takes a little longer than discharging. The current value is still constant throughout the discharge profile. This is up to the value of the limit voltage (the value of the deep discharge of the cell) at which the discharge is terminated.

4.1. LFP040AHA

The capacity characteristic (Figure 6) shows how much Ah can be sourced and need to be sunk for full charge of the battery:

- discharge = capacity of 44.815 Ah/manufacturer declares a capacity of 40 Ah.

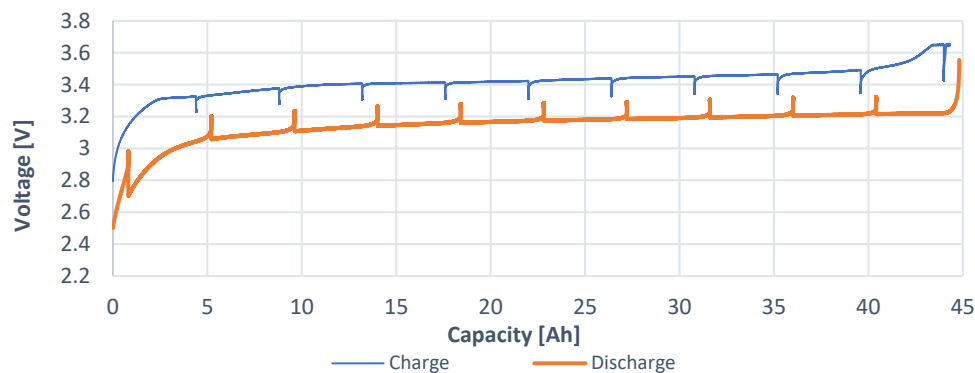


Figure 6. Charging/discharging characteristic of cell LFP040AHA as a function of capacity (relaxation periods are included).

The time characteristic (Figure 7) shows how long charging or discharging process lasts.

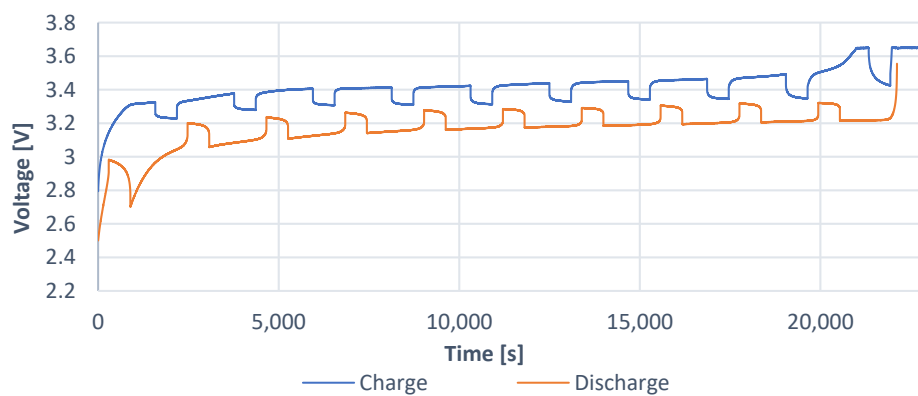


Figure 7. Charging/discharging characteristic of cell LFP040AHA as a function of time (relaxation intervals are included as well).

The OCV characteristic of cell (Figure 8) represents the voltage dependency of the cell voltage without the influence of its internal resistance. This voltage represents a DC source regarding the equivalent electrical circuit model.

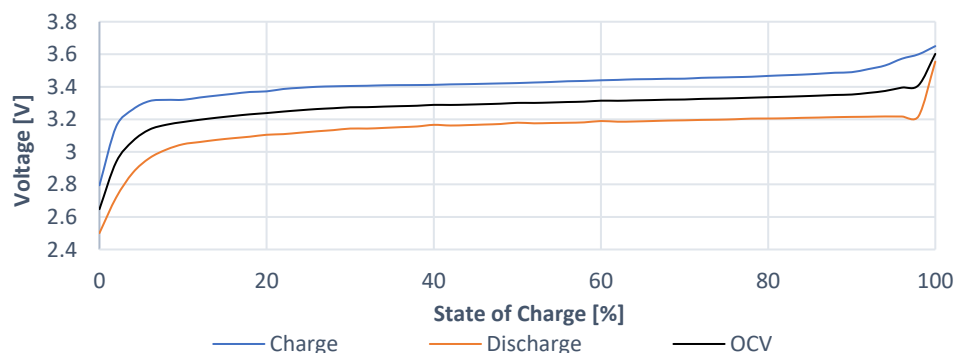


Figure 8. OCV dependency of LFP040AHA.

4.2. NPB 60 AH

As for the case of previous cell, Figure 9 represents the capacity characteristic of the second evaluated cell, i.e., it defines how much Ah can be sourced and need to be sunk for full charge of the battery:

- discharge = capacity of 62.557 Ah/manufacturer declares a capacity of 60 Ah.

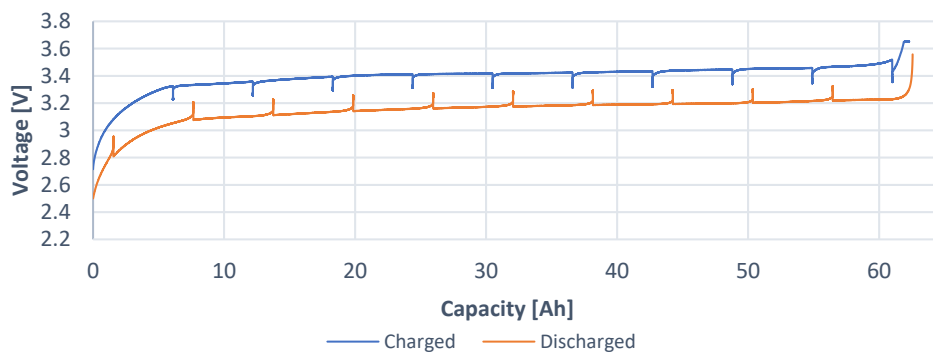


Figure 9. Voltage characteristic of cell NPB 60 AH as a function of capacity (with pauses).

The time characteristic (Figure 10) shows how long the charging or discharging process lasts.



Figure 10. Voltage characteristic of cell NPB 60 AH as a function of time (with pauses).

The OCV characteristic (Figure 11) represents the waveform of the cell voltage in the range from 0% to 100%. A higher order polynomial from this characteristic is also used within the design of EECM to represent this waveform. If compared to the waveform of previous cell, it is clear that the waveform of charging voltage characteristic and the waveform of discharging voltage characteristic is narrower. It is then clear that the internal resistance of this cell is smaller. This is further confirmed within next analyses.

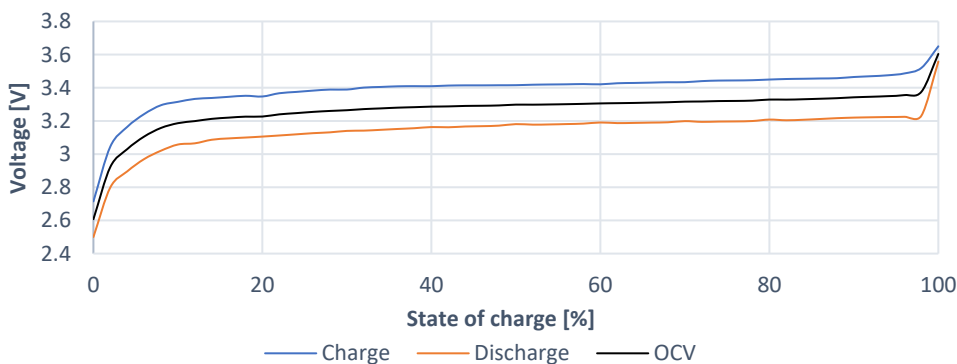


Figure 11. Voltage characteristic of cell NPB 60 AH as a function of time (with pauses).

4.3. Definition of the Values of Equivalent Electrical Schematic Model

The procedure of the identification of component values of the equivalent circuit schematic was addressed, as described above in paragraph II.B. Identification is closely related to analysis of the voltage waveforms during relaxation periods. From the first

period, the first value is found, which is relevant for 0% to 10% of SOC. The analysis follows, until the last relaxation period is reached, which represents a value ranging for 90% to 100% of SOC. From these analyzes, the dependency of the values of R_S , R_1 , R_2 , C_1 , and C_2 on the SOC are obtained.

4.3.1. LFP040AHA

Figure 12 shows graphical dependency of the values of resistances on SOC. It is seen that the change of R_1 and R_2 values is much higher compared to the value of R_S , which represents the internal resistance of the cell and is mostly constant within the whole range of SOC. Specifically, the value of the series' internal resistance is approximately $R_S = 0.007489 \Omega$. Resistance values of R_1 and R_2 are a result of the relaxation period voltage waveform shape. Therefore, during charging or discharging, the pulse-step is higher in the range from 0% to 10% than within the range from 10% to 100% SOC.

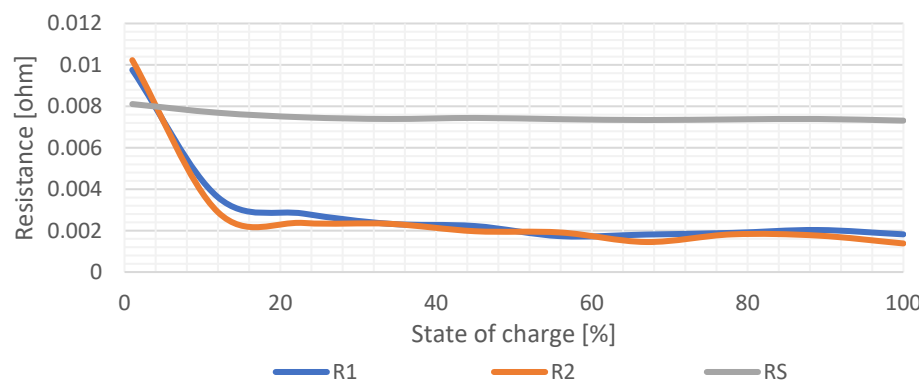


Figure 12. The waveform of internal resistance change depending on SOC LFP040AHA.

The change of the values of internal capacitive elements within the range from 0% to 100% SOC is shown in Figure 13. These capacitive elements are responsible for the relaxation durations of the voltage waveform until the OCV level is achieved. Dependency of C_1 and C_2 is similar considering shape of the waveform, while C_1 achieves higher values within whole SOC range.

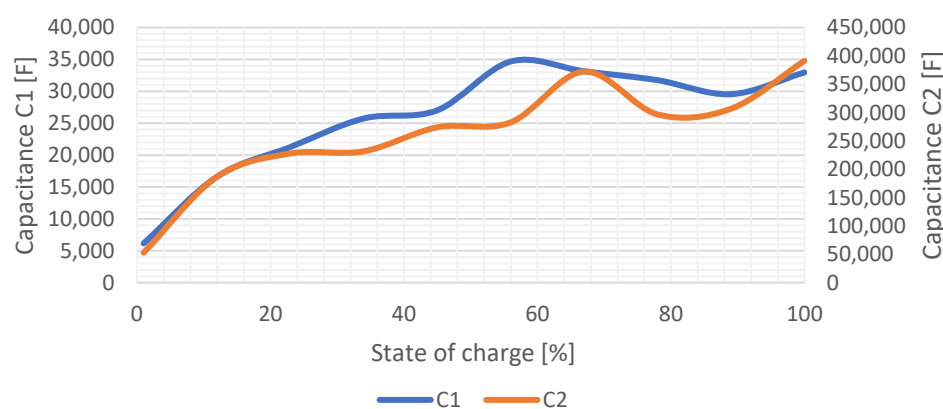


Figure 13. The waveform of capacitance change depending on SOC LFP040AHA.

4.3.2. NPB 60 AH

In the case of the NPB 60 AH cell, it can be said that the value of the internal resistance (Figure 14) compared to the LFP040AHA cell is about one-half lower. The same situation could be observed for SOC dependency of R_1 and R_2 values. From these results, it is visible that the resistive components of EECM of this cell have lower dependency on the SOC.

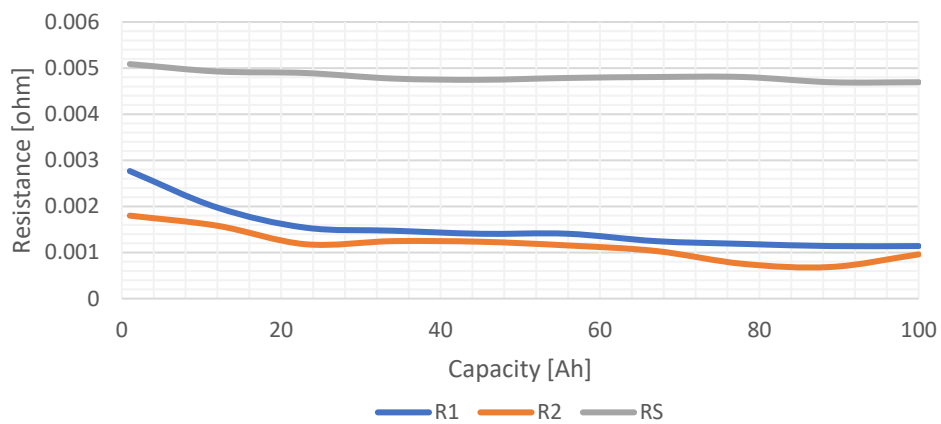


Figure 14. The waveform of internal resistance change depending on SOC NPB 60 AH.

The SOC dependency of the values of EECM capacitances of the NPB 60 AH cell is shown in Figure 15. Based on the shape of this characteristic, it can be said that these waveforms are almost linear for a certain part of the SOC. In the case of element C_1 , the characteristic exhibits a linear shape from 21,000 F to 52,000 F, while in the case of C_2 , a linear region can be detected from 300,000 F to about 600,000 F.

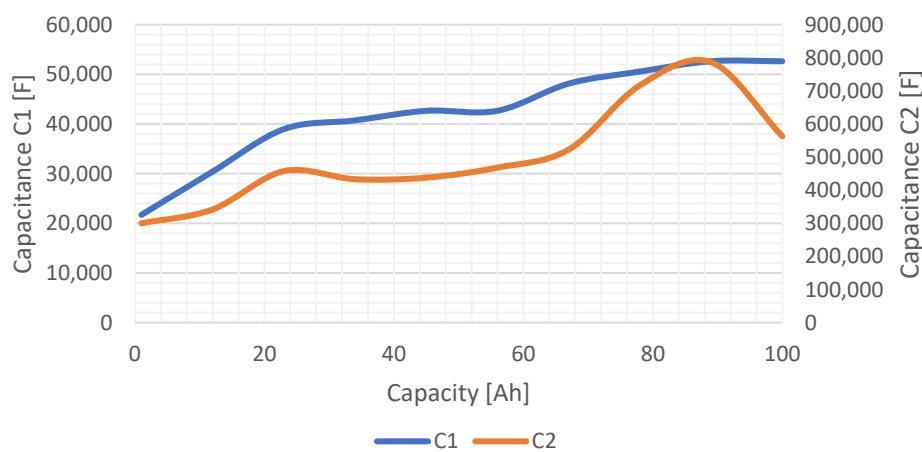


Figure 15. The waveform of capacitance change depending on SOC NPB 60 AH.

4.4. Simulation Model of the Investigated EECM of Selected Cells

4.4.1. Simulation Description

The simulation model was developed with the use of PLECS environment. This software is suitable for simulation analyses of high-performance electronic systems. Based on the previous measurements, values of the EECM have been identified in dependency on SOC (Equations (10)–(21)) and defined within simulation model (Figure 16). The simulation model is divided into two basic parts: the power part (electrical) and the computational part. The power part consists of a controlled DC power supply, passive elements R_S , R_1 , R_2 , C_1 , and C_2 , and terminals + and -. This part represents the electrical parameters of the cell simulation model. The calculation part consists of SOC calculation of the cell from the current flowing through the cell. From the SOC value, the values of components of EECM are determined. The SOC calculation is realized with the use of the Coulomb method (9).

$$SOC = SOC_{INIT} + \frac{1}{CAP_{BAT}} \int i dt \quad (9)$$

$$OCV = 2673.64u^9 - 12,284.05u^8 + 23,900.11u^7 - 25,643.65u^6 + 16,560.7u^5 - 6597.029u^4 + 15,992.14u^3 - 225.0369u^2 + 17,031.25u + 2.657236 \quad (10)$$

$$R_S = -0.003448634u^3 + 0.006592700u^2 - 0.003960356u + 0.008115255 \quad (11)$$

$$R_1 = -0.2794942u^5 + 0.7930996u^4 - 0.8393956u^3 + 0.4113761u^2 - 0.09441068u + 0.010593 \quad (12)$$

$$R_2 = -0.3810706u^5 + 1.078258u^4 - 1.132182u^3 + 0.5423415u^2 - 0.1172983u + 0.01125828 \quad (13)$$

$$C_1 = 936,076.1u^5 - 2,289,713u^4 + 198,2998u^3 - 771,318.9u^2 + 170,508.7u + 4473.228 \quad (14)$$

$$C_2 = 16,074,610u^5 - 40,537,580u^4 + 36,693,700u^3 - 14,562,760u^2 + 2,698,367u + 25,222.80 \quad (15)$$

$$OCV = 2694.048u^9 - 12,207.1u^8 + 23,428u^7 - 24,826.07u^6 + 15,878.24u^5 - 6296.461u^4 + 1532.498u^3 - 219.3959u^2 + 17.19136u + 2.620535 \quad (16)$$

$$R_S = -0.001712398u^3 + 0.003015855u^2 - 0.001733545u + 0.005106108 \quad (17)$$

$$R_1 = -0.005437838u^3 + 0.01059453u^2 - 0.006838994u + 0.00274494 \quad (18)$$

$$R_2 = 0.03354037u^5 - 0.06802538u^4 + 0.04135187u^3 - 0.005020223u^2 - 0.002721190u + 0.00184524 \quad (19)$$

$$C_1 = 51,511.30u^3 - 104,751.4u^2 + 85,594.04u + 21,625.57 \quad (20)$$

$$C_2 = -2.5671190u^5 + 5.4785070u^4 - 3.8254680u^3 + 9,603,469u^2 - 200,285.5u + 297,908.4 \quad (21)$$

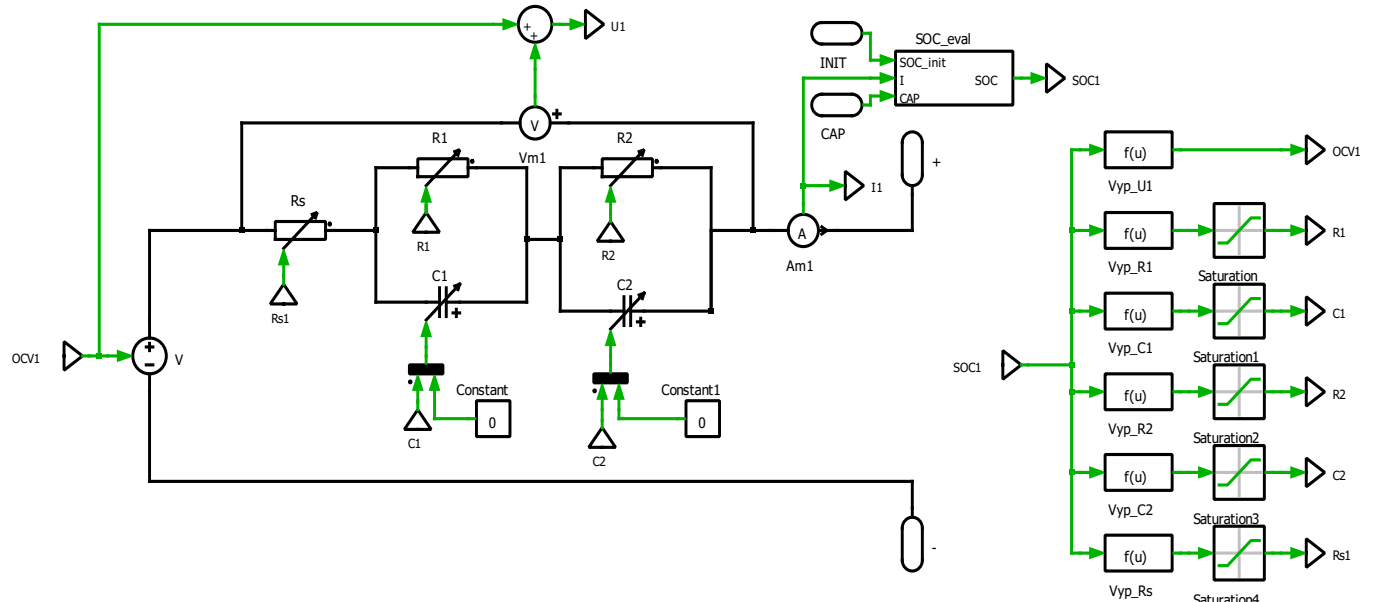


Figure 16. Proposed simulation model of selected cells using EECM.

The PLECS environment allows the design of a simple subsystem. This cell subsystem looks like the one shown in Figure 17. Two control values enter this system. One value represents the battery capacity, and the second the initial state of the charge reflecting the range from 0 to 1. Two terminals + and – come from this subsystem. These terminals represent cell terminals (anode and cathode of battery). By connecting more such cells in series-parallel, it is possible to evaluate more complex energy storage systems, i.e., high-voltage batteries.

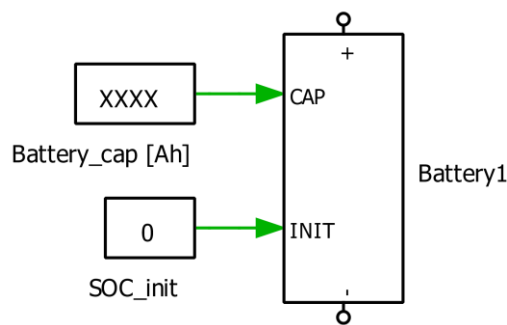


Figure 17. Battery simulation model (subsystem).

4.4.2. Simulation Results

For the LFP040AHA cell, the simulation results of the charging process are shown in Figure 18 together with the results of the discharging process. Pulse changes of SOC are visible as well, which are used for the purposes of identification of the OCV values. This value represents the real value of the voltage at the cell terminals. The internal resistance and parameters of the RC cell are reflected here.

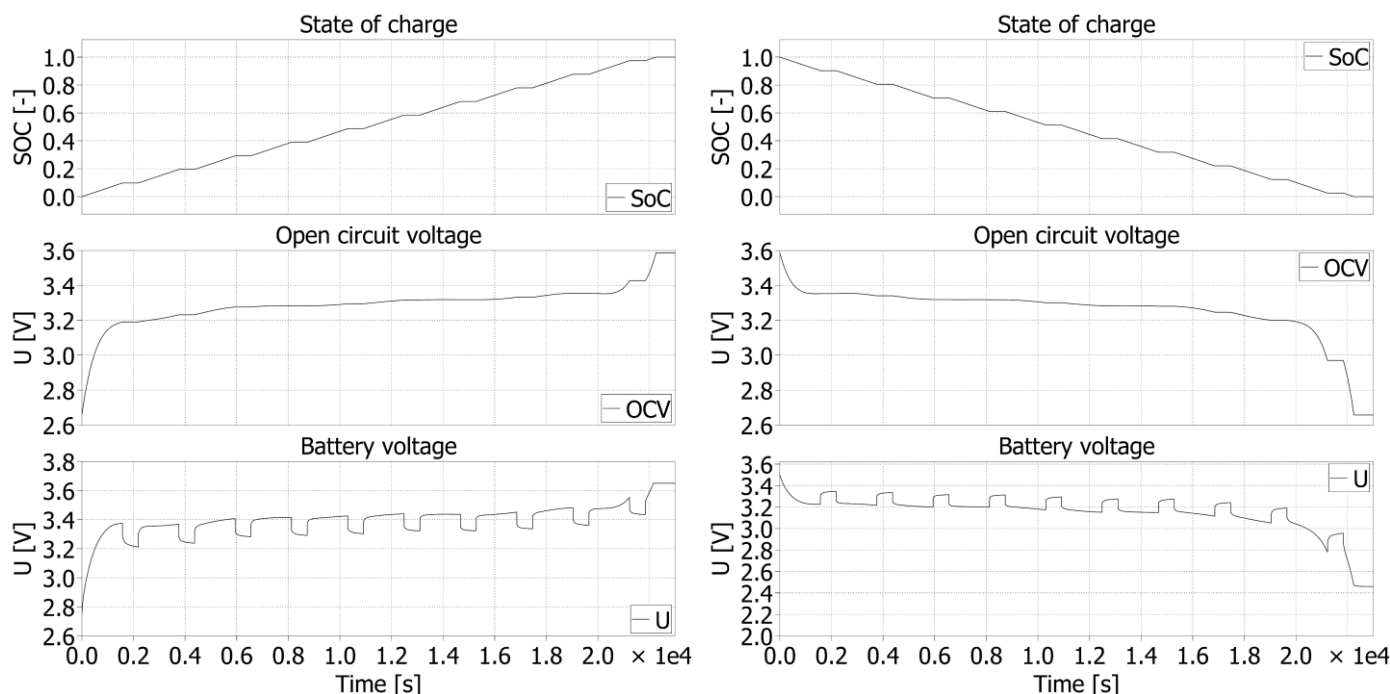


Figure 18. LFP040AHA—Simulation result of the charging process (left) and discharging process (right).

Similar results are simulated for NPB 60 AH. The waveforms referring to the charging and discharging are shown in Figure 19. Three variables are evaluated as in the previous case to determine OCV waveform.

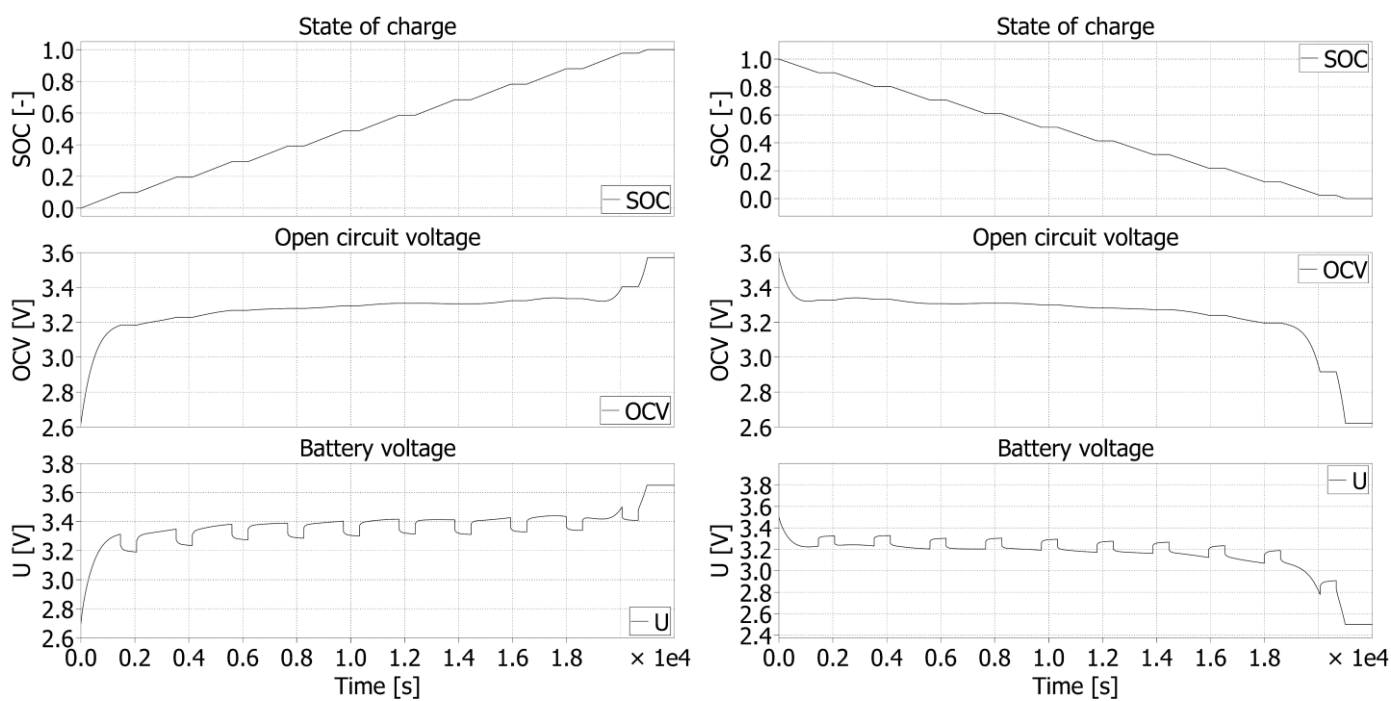


Figure 19. NPB 60 AH—Simulation result of the charging process (**left**) and discharging process (**right**).

5. Comparison of the Simulation Results with Experimental Measurements

The resulting waveforms, which are mutually compared, refer to the charging and discharging process of selected cells. In order to evaluate the accuracy of the presented identification methodology and simulation modelling, the relative error between simulation and experimental measurement is evaluated. The value of relative error is higher at the beginning and at the end of these processes. Basically, the highest achieved value targets 5% of relative error for the regions is around 10% and 90% of SOC. Within the range of 20–80% of SOC, the error achieves approximately 2%.

5.1. Charging and Discharging Cells

5.1.1. LFP040AHA

In the first case, pulse charging and discharging of the LFP040AHA cell is displayed. These waveforms are shown in Figure 20. The red waveform represents the real measured values, and the blue cell represents the result of the discharge simulation of the LFP040AHA cell. It is clear from the figure that this model is accurate enough for use in complex applications consisting of these articles.

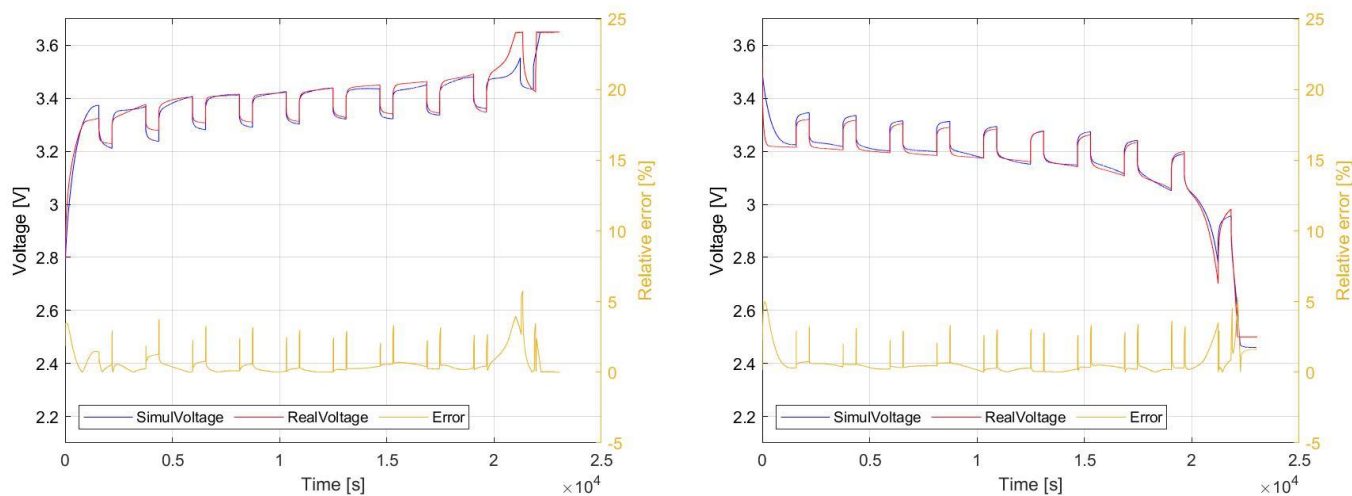


Figure 20. Comparison of simulation results with experimental results for charging (left) and discharging (right) for LFP040AHA.

5.1.2. NPB 60 AH

As in the previous case, Figure 21 shows a comparison of the pulse charging and discharging waveforms of the NPB 60 AH. If we consider the evaluation of the relative error, comparing to previous case, a more stable accuracy and lower relative error values are achieved. For the most of the SOC range, the relative error is no more than 1%.

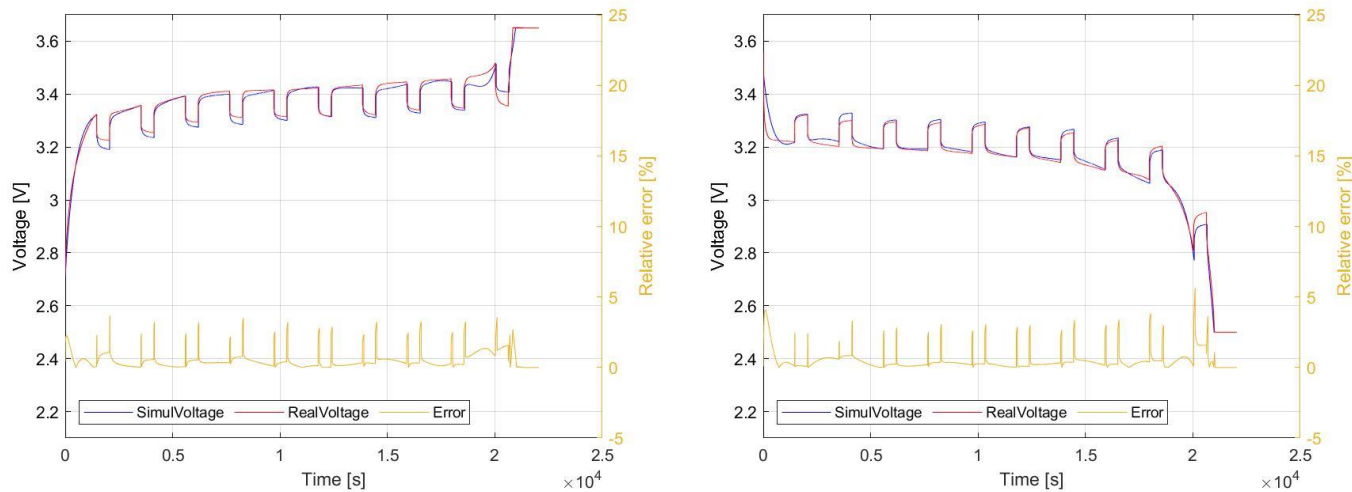


Figure 21. Comparison of simulation results with experimental results for charging (left) and discharging (right) for NPB 60 AH.

5.2. Comparisons of the Values of Components of EECM, Simulation vs. Measurements

The comparison of the parameters of the equivalent replacement scheme of the cell was performed as a comparison of the waveforms of the measured parameters OCV , R_S , R_1 , R_2 , C_1 , and C_2 with the simulated results.

Figure 22 shows the OCV waveform of the LFP040AHA and NPB 060AH cells from Figure 8. The measured results are represented by red waveform, while blue refers to simulation results achieved as polynomial formula (2). This polynomial almost completely overlaps the measured waveform, so the model in terms of OCV represents a highly accurate system.

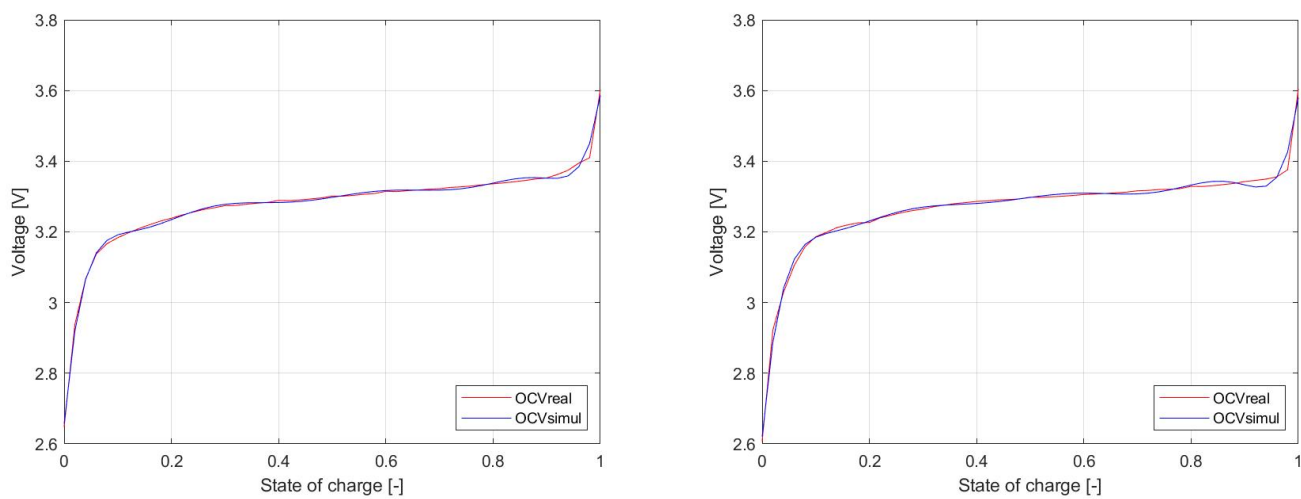


Figure 22. Comparison of OCV dependency of EECM and real cell (LFP040AHA—left, NPB 060 AH—right).

Figure 23 shows comparisons of the dependency of resistive elements of EECM. Experimental waveforms were initially represented on Figure 12, while here they are compared to simulation. Green waveforms refer to R_S , red waveforms represent dependency of R_1 , and blue waveforms are related to R_2 .

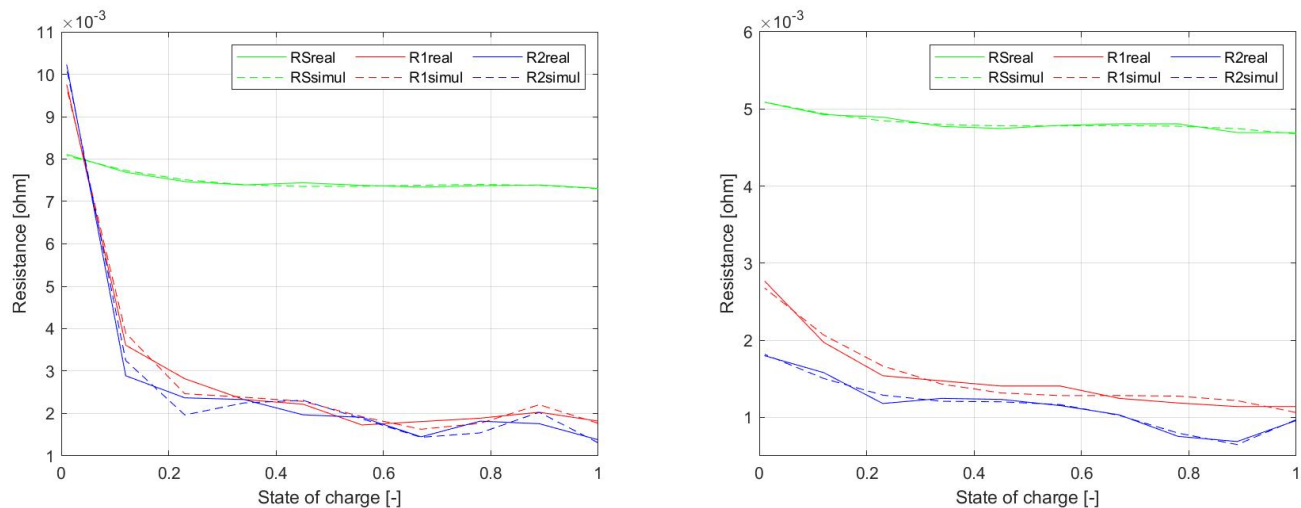


Figure 23. Comparison of dependency of resistive elements of EECM and real cell (LFP040AHA—left, NPB 060 AH—right).

Figure 24 shows dependency of the values of capacitive elements of EECM. As in the previous case, the solid lines refer to the measured data, while dashed lines refer to the simulation results. It appears that simulation model reliably follows the behavior of the cell itself.

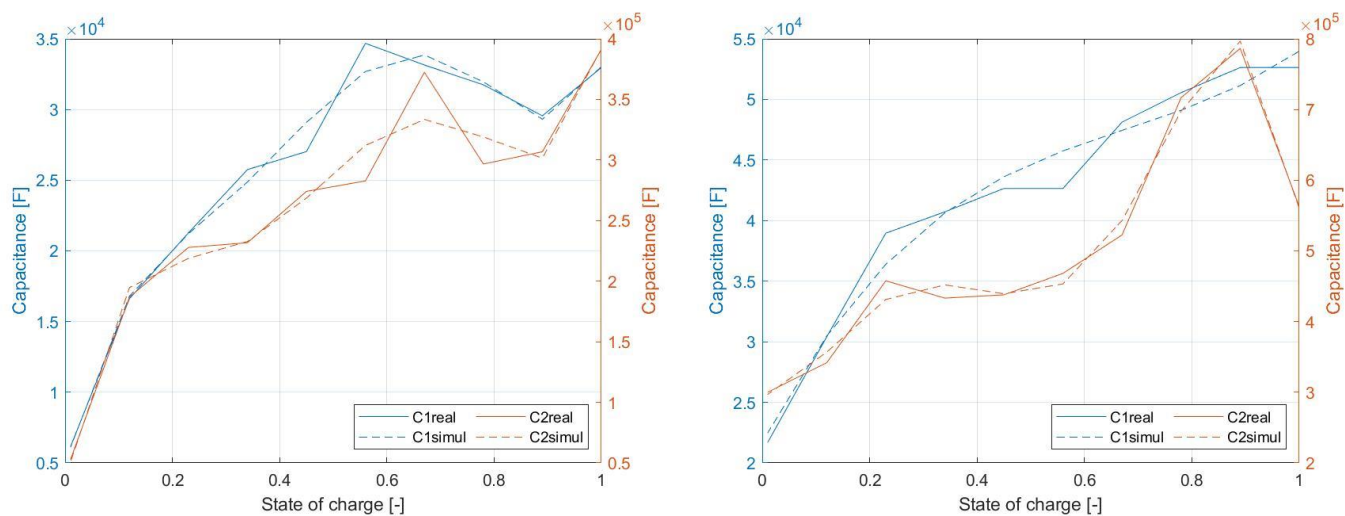


Figure 24. Comparison of dependency of capacitive elements of EECM and real cell (LFP040AHA—left, NPB 060 AH—right).

6. Conclusions

The article described the motivation for development of a system used for identification of the equivalent electrical schematic model of a battery. Insufficient descriptions of the parameters given by the manufacturers of electrochemical cells leads to the need for utilization of the presented methodology in order to be able to determine the values of components which are required for battery modeling. These are OCV, R_S , R_1 , R_2 , C_1 , and C_2 parameters and their dependency on the SOC. The presented modelling approach enables to identify the simulation model, which is capable of representing the dynamic performance of cells, while its complexity offers the possibility to model complex battery modules and battery packs. In this way, complex energy storage systems can be designed and investigated under the operation of various power electronic systems.

Using an algorithm in the LabView environment, a programmable load and a programmable source were controlled. The discharging/charging profile was set by this algorithm, and the parameters of the EESM were determined from the measurement results of these discharging/charging profiles. These elements are represented mathematically using higher order polynomials. The polynomials contain a dependency of these parameters on the change in the current SOC of the electrochemical cell. These changes range from 0 to 1 SOC.

From the measurements, it was found that the manufacturer produces two types of cells that are relatively the same. In the analysis of these cells, it was found that these cells have very different values of the internal elements EESM. Although these cells are of the same type of LiFePO₄ cathode material, they are very different. This difference is not declared in any datasheet from the manufacturer. This difference in the internal parameters of the replacement equivalent scheme was demonstrated by the fact that these cells cannot be loaded with the same value of load current C. Due to the difference in these parameters, there was the problem that when discharging the NPB 60 AH cell with a value of 3 C (180 A) for the cell, the cell temperature reached 45–50 °C after termination. While in the case of the LFP040AHA cell, which was also loaded with a value of 3 C (120 A) for the given cell, the temperature after termination reached up to 60 °C. This small invisible difference in these cells could cause major system heat dissipation problems to system developers in sharp applications. This temperature difference at the same load is mainly due to the R parameters from the replacement equivalent cell scheme.

In terms of the simulation model, it can be said that the model shown above in the cell corresponds to real samples. Of course, the algorithm can set the measurement of any cell. It is enough to enter the parameters necessary for measuring different cells into the algorithm, and this can ensure the measurement of different types of cells. From these

measurements, it is possible to determine any alternative equivalent scheme from the article. Based on the measurements and data analysis shown above, it is possible to construct a simulation model for different types of cells.

When comparing real and measured waveforms, this simulation model corresponds sufficiently to the real cell in both cases. This cell is suitable for more complex simulations in the field of smart grid, electromobility, testing of balancing systems, or renewable energy storage.

Author Contributions: Conceptualization, methodology M.F., validation, formal analysis, investigation, M.S. All authors have read and agreed to the published version of the manuscript.

Funding: This research received no external funding.

Institutional Review Board Statement: Not applicable.

Informed Consent Statement: Not applicable.

Acknowledgments: This publication was realized with support of Operational Program Integrated Infrastructure 2014–2020 of the project: Innovative Solutions for Propulsion, Power and Safety Components of Transport Vehicles, code ITMS 313011V334, co-financed by the European Regional Development Fund. Authors would like to thank also to national grant agency Vega for project funding Vega-1/0063/21.

Conflicts of Interest: The authors declare no conflict of interest.

References

1. Abu-Sharkh, S.; Doerffel, D. Rapid test and non-linear model characterisation of solid-state lithium-ion batteries. *J. Power Sources* **2004**, *130*, 266–274. [[CrossRef](#)]
2. Zhang, C.; Allafi, W.; Dinh, Q.; Ascencio, P.; Marco, J. Online estimation of battery equivalent circuit model parameters and state of charge using decoupled least squares technique. *Energy* **2018**, *142*, 678–688. [[CrossRef](#)]
3. Thakkar, R.R. Electrical Equivalent Circuit Models of Lithium-ion Battery. In *Management and Applications of Energy Storage Devices*; Okedu, K.E., Ed.; InTech: London, UK, 2021.
4. Chen, W.J.; Tan, X.J.; Cai, M. Parameter identification of equivalent circuit models for Li-ion batteries based on tree seeds algorithm. *IOP Conf. Ser. Earth Environ. Sci.* **2017**, *73*, 012024. [[CrossRef](#)]
5. Eltoumi, F.; Badji, A.; Becherif, M.; Ramadan, H.S. Experimental Identification using Equivalent Circuit Model for Lithium-Ion Battery. *Int. J. Emerg. Electr. Power Syst.* **2018**, *19*, 20170210. [[CrossRef](#)]
6. Mesbahi, T.; Rizoug, N.; Bartholomeus, P.; Sadoun, R.; Khenfri, F.; Le Moigne, P. Dynamic Model of Li-Ion Batteries Incorporating Electrothermal and Ageing Aspects for Electric Vehicle Applications. *IEEE Trans. Ind. Electron.* **2018**, *65*, 1298–1305. [[CrossRef](#)]
7. Agudelo, B.; Zamboni, W.; Monmasson, E.; Spagnuolo, G. Identification of battery circuit model from EIS data. *JCGE Congrès Des Jeunes Cherch. En Génie Electr.* **2019**. Available online: <https://hal.archives-ouvertes.fr/hal-02915697/document> (accessed on 19 January 2022).
8. Hruska, K.; Kindl, V.; Pechanek, R.; Skala, B. Evaluation of Different Approaches of Mathematical Modelling of Thermal Phenomena Applied to Induction Motors. In Proceedings of the 2014 ELEKTRO, Rajecke Teplice, Slovakia, 19–20 May 2014; pp. 358–362. [[CrossRef](#)]
9. Scrosati, B. History of lithium batteries. *J. Solid State Electrochem.* **2011**, *15*, 1623–1630. [[CrossRef](#)]
10. Yoo, H.D.; Markevich, E.; Salta, G.; Sharon, D.; Aurbach, D. On the challenge of developing advanced technologies for electrochemical energy storage and conversion. *Mater. Today* **2014**, *17*, 110–121. [[CrossRef](#)]
11. Daowd, M.; Omar, N.; Bossche, P.V.D.; Van Mierlo, J. Passive and active battery balancing comparison based on MATLAB simulation. In Proceedings of the 2011 IEEE Vehicle Power and Propulsion Conference, Chicago, IL, USA, 6–9 September 2011; ISBN 978-1-61284-247-9. [[CrossRef](#)]
12. Chamnan-arsa, S.; Uthaichana, K.; Kaewkham-ai, B. Modeling of LiFePO₄ battery state of charge with recovery effect as a three-mode switched system. In Proceedings of the 2014 13th International Conference on Control, Automation Robotics & Vision (ICARCV), Singapore, 10–12 December 2014; pp. 1712–1717. [[CrossRef](#)]
13. Filkusová, M.; Fedorková, A.; Oriňáková, R.; Oriňák, A.; Nováková, Z.; Škantárová, L. Effect of multi-walled carbon nanotubes on the thermal stability and surface morphology of LiFePO₄ cathode material. *New Carbon Mater.* **2013**, *28*, 1–7. [[CrossRef](#)]
14. Chiu, H.-J.; Lin, L.-W.; Pan, P.-L.; Tseng, M.-H. A novel rapid charger for lead-acid batteries with energy recovery. *IEEE Trans. Power Electron.* **2006**, *21*, 640–647. [[CrossRef](#)]
15. National Instruments, NI PXI-1031 User Manual. Available online: <https://www.ni.com/pdf/manuals/371226g.pdf> (accessed on 19 January 2022).
16. KIKUSUI. Multifunctional Electronic Load PLZ-4W Series. Available online: <https://kikusui.co.jp/en/product/detail.php?IdFamily=0011> (accessed on 19 January 2022).

17. Elektro-Automatik, EA-PSI 8000 2U 640W–3000W, Programmable Laboratory Power Supplies. Available online: <https://elektroautomatik.com/shop/en/products/programmable-dc-laboratory-power-supplies/discontinued-series/series-psi-8000-2u-br-640-w-up-to-3-kw/> (accessed on 19 January 2022).
18. Boukhal, M.A.; Lagrat, I.; Elbannay, O. Implementation of a lithium-ion battery state of charge estimation algorithm for BMS on the real time target NI myRio. In Proceedings of the 2019 International Conference on Wireless Technologies, Embedded and Intelligent Systems (WITS), Fez, Morocco, 3–4 April 2019; pp. 1–5. [CrossRef]
19. Cacciato, M.; Nobile, G.; Scarella, G.; Scelba, G.; Sciacca, A.G. Energy management optimization in stand-alone power supplies using online estimation of battery SOC. In Proceedings of the 2016 18th European Conference on Power Electronics and Applications (EPE'16 ECCE Europe), Karlsruhe, Germany, 5–9 September 2016; pp. 1–10. [CrossRef]
20. Kazda, T.; Capková, D.; Jašo, K.; Straková, A.F.; Shembel, E.; Markevich, A.; Sedlaříková, M. Carrageenan as an Ecological Alternative of Polyvinylidene Difluoride Binder for Li-S Batteries. *Materials* **2021**, *14*, 5578. [CrossRef] [PubMed]
21. Cacciato, M.; Nobile, G.; Scarella, G.; Scelba, G. Real-time model-based estimation of SOC and SOH for energy storage systems. In Proceedings of the 2015 IEEE 6th International Symposium on Power Electronics for Distributed Generation Systems (PEDG), Aachen, Germany, 22–25 June 2015; pp. 1–8. [CrossRef]
22. Gwl Power. Technical Specification, Datasheet Winston LFP040AHA Cell. Available online: https://files.gwl.eu/inc/_doc/attach/StoItem/1123/GWL-Winston-LFP040AHA.pdf (accessed on 19 January 2022).
23. Gwl Power. Technical Specification, Datasheet NPB60AH, NPB100AH. Available online: https://files.gwl.eu/inc/_doc/attach/StoItem/4184/NPB60AH_NPB100AH_Datasheet.pdf (accessed on 19 January 2022).
24. Battery University. Available online: <https://batteryuniversity.com/> (accessed on 19 January 2022).